

Low Thermal Expansion of $\text{Ba}_{0.5}\text{Sr}_{0.5}\text{Co}_{0.7}\text{Fe}_{0.2}\text{Mn}_{0.1}\text{O}_{3-\delta}$ cathode Material

Dechuan Li*, Yongxing Zhang, Guangping Zhu, Xude Wang

School of Physics and Electronic Information, Huaibei Normal University, Huaibei, 235000, China

*E-mail: dchli@qq.com

Received: 4 March 2018 / Accepted: 9 April 2018 / Published: 10 May 2018

Low thermal expansion $\text{Ba}_{0.5}\text{Sr}_{0.5}\text{Co}_{0.7}\text{Fe}_{0.2}\text{Mn}_{0.1}\text{O}_{3-\delta}$ (BSCFM-0.1) material was prepared to improve the thermal compatibility between cathode and electrolyte for intermediate temperature solid oxide fuel cells. The pure perovskite BSCFM-0.1 can be obtained by a combined citrate and EDTA complexing method. The results show that Mn was introduced to replace Co in B-site of $\text{Ba}_{0.5}\text{Sr}_{0.5}\text{Co}_{0.8}\text{Fe}_{0.2}\text{O}_{3-\delta}$ (BSCF) to depress thermal expansion. Thermal expansion coefficient of BSCFM-0.1 is $14.24 \times 10^{-6} \text{ K}^{-1}$ at 600°C , and $14.97 \times 10^{-6} \text{ K}^{-1}$ at 700°C , respectively. It is a smaller value comparing with BSCF for $15.62 \times 10^{-6} \text{ K}^{-1}$ at 600°C and $16.76 \times 10^{-6} \text{ K}^{-1}$ at 700°C . The small difference of thermal expansion is helpful for cathode adhering to the ceria-base electrolyte. As to the single cell, the maximum power density is 110 mW cm^{-2} at 600°C , which is slightly higher than that of BSCF cathode (102 mW cm^{-2} at 600°C). The results imply that the rate of lattice oxygen release has been slowed down to control the concentration of oxygen vacancies in the lattice by Mn partial substitution without reducing electrical properties. The gradual increase of thermal expansion is beneficial to improve the thermal compatibility between cathode and electrolyte for SOFCs.

Keywords: Electrode materials; Cathode; Thermal expansion; Electrochemical performance; SOFCs

1. INTRODUCTION

Perovskite oxide ($\text{Ba}_{0.5}\text{Sr}_{0.5}\text{Co}_{0.8}\text{Fe}_{0.2}\text{O}_{3-\delta}$) is an attractive mixed conductor with the oxygen ion and electronic conduction for solid oxide fuel cells [1-6]. Oxygen vacancies are created by the introduction of low valence metal ion into A-sites for the oxygen ionic conductivity [7, 8]. As for B-sites, the electron can be transferred among the metal ions for electron conduction. However, when the temperature increases, B-site ion will be reduced. The reduction increases the concentration of oxygen vacancy by the loss of lattice oxygen. The concentration of oxygen vacancies is closely related to electrical conductivity and thermal expansion. In addition, thermal compatibility is also a critical factor for the lifetime of fuel cells. The mismatch of thermal expansion between cathode and electrolyte

usually causes completely damage of cell especially for the larger different of thermal expansion coefficient. If the cathode material expansion coefficient is closed to ceria-base electrolyte, the cathode could be directly sintered with electrolyte to avoid the redundant phase existing in the grain boundary to improve the oxygen ionic conduction. Hence, low expansion cathode material should be discussed. As report that positive or negative charge concentration and their relative distance in the lattice are related to the character of thermal expansion [9]. Shao investigates the relationship between doped metal ions in A-site and thermal expansion in $\text{Ba}_x\text{Sr}_{1-x}\text{Co}_{0.8}\text{Fe}_{0.2}\text{O}_{3-\delta}$ and concludes that $\text{Ba}_{0.5}\text{Sr}_{0.5}\text{Co}_{0.8}\text{Fe}_{0.2}\text{O}_{3-\delta}$ has less thermal expansion coefficient (TEC) when $x=0.5$ [10]. Tietz et al. [11] studied the kind of B-site element on the effect of thermal expansion of $\text{La}_{1-x}\text{Sr}_x\text{MeO}_3$ (Me=Mn, Co, Fe) perovskite series. Their results showed that $\text{La}_{0.8}\text{Sr}_{0.2}\text{MnO}_{3-\delta}$ has the lowest TEC value ($11.80 \times 10^{-6} \text{ K}^{-1}$) than that of $\text{La}_{0.8}\text{Sr}_{0.2}\text{CoO}_{3-\delta}$ ($19.10 \times 10^{-6} \text{ K}^{-1}$) and $\text{La}_{0.8}\text{Sr}_{0.2}\text{FeO}_{3-\delta}$ ($12.20 \times 10^{-6} \text{ K}^{-1}$) for SOFCs. It indicated that Mn is a selective element in decreasing the thermal expansion of cathode. However, $\text{La}_{0.8}\text{Sr}_{0.2}\text{MnO}_{3-\delta}$ material is usually used for the high temperature SOFCs because the oxygen ion conductivity can be sufficiently activated only in the high temperature [12, 13]. As for intermediate temperature SOFCs, BSCF is an attractive material for its high oxygen vacancy diffusion rate, oxygen permeability, oxygen adsorption/desorption except for the large thermal expansion ($20.00 \times 10^{-6} \text{ K}^{-1}$) [14-16]. Mn ion have more different valence in the oxidation-reduction reaction. The difference between radius values of Mn ion adjacent valence is greater than that of Co ion. The greater the difference values, the more difficult the reduction reaction of Mn ion in the lattice. The large difference of ionic radius depressed the thermal expansion in relatively low temperature. When the temperature is increased, the Mn ion could be activated for the transmission of electrons.

On the other hand, multivalent metal ions in B-sites of perovskite material usually have high TEC because of the reduction of high oxidation state especially for Co^{4+} [17]. In order to increase the thermal compatibility of the cell component, the large TEC should be decreased. Therefore, the multivalent Mn ion was introduced to B-sites of BSCF perovskite to reduce the cathode material expansion for IT-SOFCs. In the present work, the character, thermal expansion and electrochemical performance of partial substitution for Co by Mn of $\text{Ba}_{0.5}\text{Sr}_{0.5}\text{Co}_{0.8-x}\text{Fe}_{0.2}\text{Mn}_x\text{O}_{3-\delta}$ cathode materials were investigated.

2. EXPERIMENTAL

2.1 Materials and Methods

$\text{Ba}_{0.5}\text{Sr}_{0.5}\text{Co}_{0.8}\text{Fe}_{0.2}\text{O}_{3-\delta}$ (noted as BSCF) and $\text{Ba}_{0.5}\text{Sr}_{0.5}\text{Co}_{0.8-x}\text{Fe}_{0.2}\text{Mn}_x\text{O}_{3-\delta}$ ($x= 0.1, 0.2, 0.3$) (BSCFM-x) powders were synthesized by a combined citrate and EDTA complexing method [15]. All the nitrate salts, $\text{Ba}(\text{NO}_3)_2$, $\text{Sr}(\text{NO}_3)_2$, $\text{Co}(\text{NO}_3)_2 \cdot 6\text{H}_2\text{O}$, $\text{Fe}(\text{NO}_3)_3 \cdot 9\text{H}_2\text{O}$ and $\text{Mn}(\text{NO}_3)_2 \cdot 6\text{H}_2\text{O}$, were dissolved in the mixed EDTA and NH_4OH solution. When the nitrate salts were completely mixed, the citric acid as a complexing reagent was added into the solution. The ratio was set to 1:1:1.5 for metal ions: EDTA: citric acid. Then the mixed solution was stirred at 80°C . Finally, the gel is formed. When the gel was dried, the precursor was calcinated at different temperatures to obtain the target compound.

2.2 Characterizations

In the TEC measurement, the cathode samples were sintered to a compact cylinder with the dimensions of $\Phi 11 \times 4$ mm³ for BSCF and BSCFM-0.1. Two samples were fired at 1100°C for 4h, the finally densities were higher than 94% of the theoretical value as measured by the Archimedes method. At the same times, La doped ceria electrolyte Ce_{0.82}La_{0.18}O_{2- δ} (LDC) was prepared by solid phase reaction [18]. The single cell is fabricated with LDC electrolyte (1.5 mm thickness and 11 mm diameter), BSCFM-x cathode (120 μ m thickness) and NiO (50 wt%)+LDC(50 wt%) anode (100 μ m thickness) for the output performance test, which is described detailedly in the literature [19]. The effective electrode area was 0.50 cm². On the cell performance test, the cathode was exposed to air, and the anode side was exposed to 3% H₂O + humidified H₂ at a constant flowing rate of 50 ml min⁻¹.

The crystal structures of powders were characterized by X-ray diffraction (PANalytical B.V.) using an X'pert PRO diffractometer and Cu K α radiation in the 2 Θ range of 10-80°. Scanning electron microscopy (SEM) (JSM-6700F) and energy dispersive spectrometry (EDS) were employed to examine the morphology and element distribution of the sample. The linear thermal expansion coefficient was measured on the thermal expansion apparatus (LINSEIS DIL L76) using quartz as the reference material with a heating rate of 5°C min⁻¹ from room temperature to 800°C. The performance of a single cell was measured by an electrochemical workstation (PARSTAT 2273, Princeton, USA).

3. RESULTS AND DISCUSSION

3.1 Crystal structure of Ba_{0.5}Sr_{0.5}Co_{0.8-x}Fe_{0.2}Mn_xO_{3- δ}

Figure 1 shows the XRD patterns of Ba_{0.5}Sr_{0.5}Co_{0.7}Fe_{0.2}Mn_{0.1}O_{3- δ} precursor powder after calcination at 900, 1000, 1100°C for 4h. As can be seen, the perovskite structure of Mn-doped Ba_{0.5}Sr_{0.5}Co_{0.7}Fe_{0.2}Mn_{0.1}O_{3- δ} has been formed at 900°C. However, the secondary phases were also existed even at 1000°C. Some of extra peaks were observed around at 27.82, 29.38, 43.88 degrees of 2 Θ . The impurity phases of BaFe₂O₄ (JCPDS: 00-26-0158) and BaSrFe₄O₈ (JCPDS: 01-076-2172) were detected in the sample sintering at 900°C and 1000°C. In fact, it is easy to generate impurity phases in the process of material synthesis. Niedrig et al. also reported that the hexagonal phase might be formed after the cubic BSCF power annealing in ambient air for a long time [20]. Wang et al. investigated the intermediate process of BSCF powder by High-temperature X-ray diffraction during the cooling and heating at different oxygen partial pressure [21]. They also found the intermediate phase of BSCF was existed only in a specific environment. When the calcinated temperature increased to 1100°C, the trivial peaks almost disappear. The cubic perovskite of Ba_{0.5}Sr_{0.5}Co_{0.7}Fe_{0.2}Mn_{0.1}O_{3- δ} were obtained.

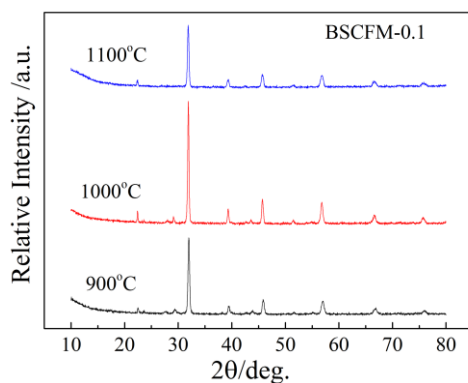


Figure 1. XRD patterns of BSCFM-0.1 calcination at 900, 1000, 1100°C for 4h.

Figure 2 shows the XRD patterns of BSCF and BSCFM- x ($x=0, 0.1, 0.2, 0.3$) powders. From the patterns, all the samples possess the perovskite structure. When the Mn addition is beyond 0.2, the extra phases such as barium iron oxide and strontium cobalt oxide were also observed. For BSCFM-0.1 oxide, the diffraction peaks shift slightly to a higher 2θ angle compared to that of BSCF. The lattice of BSCFM-0.1 is contracted under the Mn doped. It might be due to the relatively larger Co^{4+} and Co^{3+} ions substituted by the Mn^{4+} in BSCF oxide [10]. The radius of Mn^{4+} is smaller than that of Co^{3+} [22]. This contraction is useful to reduce the expansion of cathode material in matching the ceria-based electrolyte for SOFCs.

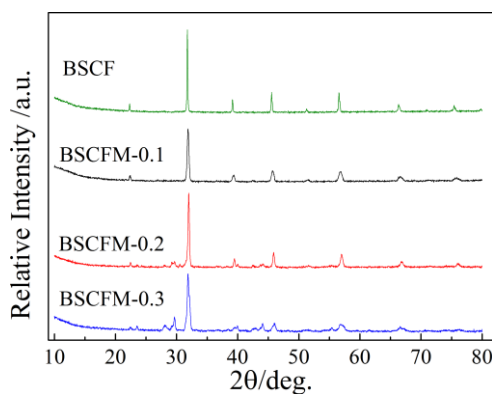


Figure 2. XRD patterns of BSCFM- x ($x=0, 0.1, 0.2, 0.3$) powders calcination at 1100°C for 4h.

3.2 Microstructure

In order to exhibit the element composition of BSCFM-0.1, the SEM-EDS micro-region analysis was taken on the surface of calcinated powder. As can be seen in Figure 3(a), the powder is fine on the whole image. The random regions were selected for the chemical composition analysis. Figure 3(b) gives the EDS pattern of BSCFM-0.1, and the precise composition is summarized in Table 1. The average chemical compositions are as follows: Ba 9.00%, Sr 9.06%, Co 13.31%, Fe 3.62% and Mn 1.49%. The ratio of A-site to B-site is close to 1 for the BSCFM-0.1 perovskite oxide. We also

examined the BSCFM-0.1 cathode material sintering at 1100°C by ICP (Agilent 7500CS), the element contents (Ba 8.95%, Sr 9.11%, Co 13.11%, Fe 3.55% and Mn 1.71%) are closed to the data, which were analyzed by Energy Dispersive Spectrometry. It might indicate the Mn is successfully added into the B-site of the perovskite structure.

Table 1 Composition of the detected elements of two random areas on the surface of BSCFM-0.1.

Element	BSCFM-0.1 (Atom (%))		Average
	Spectrum 1	Spectrum 2	
O K	62.31	64.72	63.52
Mn K	1.44	1.54	1.49
Fe K	3.80	3.44	3.62
Co K	13.87	12.75	13.31
Sr K	9.28	8.85	9.06
Ba L	9.30	8.70	9.00
Total	100.00	100.00	100.00

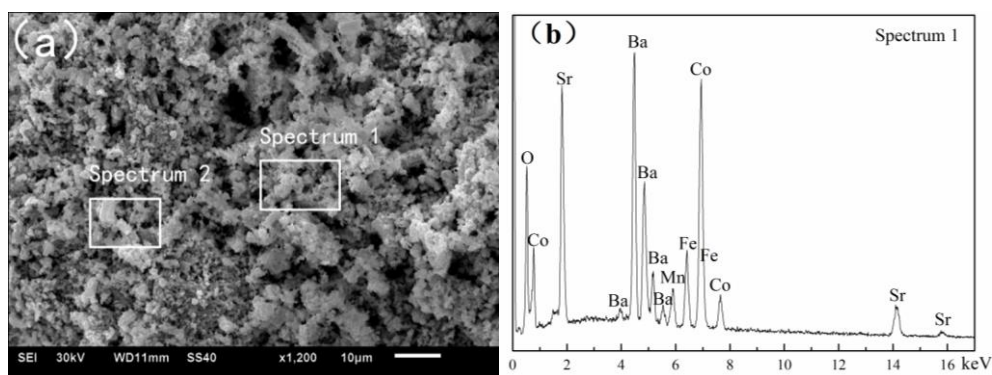


Figure 3. SEM and EDS of the BSCFM-0.1 sintered at 1100°C for 4h: (a)SEM micrograph; (b) Typical EDS spectrum of area 1.

3.3 Thermal expansion

Figure 4(a) shows the variation of relative length of BSCF and BSCFM-0.1 at a heating rate of 5°C min⁻¹ from room temperature to 800°C. The whole expansion behaviors are similar, but the thermal expansion is more gently for BSCFM-0.1 than that of BSCF in the whole temperature range. From the curve, there are two obvious inflexions around to 100 and 450°C. At the inflexion of 100°C, the appearance maybe attribute to the influence of water evaporation and gas release. The more obvious inflexion around 450°C mainly be related to the loss of the lattice oxygen followed by the thermal reductions of Co⁴⁺/Fe⁴⁺ to Co³⁺/Fe³⁺ in B-site [23].

The corresponding values of thermal expansion coefficient (TEC) are shown in Figure 4(b). As can be seen, the value of BSCF TEC is decreased as the Mn doped. The curve of BSCFM-0.1 is raised more slowly than that of BSCF when the temperature increased from 200°C to 800°C. The slower the

TEC increased, the better the cathode tightly adheres to the electrolyte. The TEC of BSCFM-0.1 is $14.24 \times 10^{-6} K^{-1}$ at $600^\circ C$, $14.65 \times 10^{-6} K^{-1}$ at $650^\circ C$ and $14.97 \times 10^{-6} K^{-1}$ at $700^\circ C$, respectively. The values were lower than that of BSCF. Li reported that the TEC of Gd doped $(Ba_{0.7}Sr_{0.3})_{0.95}Gd_{0.05}Co_{0.8}Fe_{0.2}O_{3-\delta}$ have the minimum TEC value ($19.80 \times 10^{-6} K^{-1}$) between 50 and $800^\circ C$ [24]. The TEC value of Sm doped $(Ba_{0.5}Sr_{0.5})_{1-x}Sm_xCo_{0.8}Fe_{0.2}O_{3-\delta}$ are between 19.50 and $20.10 \times 10^{-6} K^{-1}$ from 30 to $800^\circ C$ [25]. However, the expansion of Mn doped BSCFM-0.1 cathode material is more closed to ceria-based electrolyte, such as SDC and GDC ($12.20 \times 10^{-6} K^{-1}$ [26]) for intermediate temperature solid oxide fuel cells. It could be concluded that this low expansion cathode material could enhance the thermal compatibility between cathode and ceria-based electrolyte.

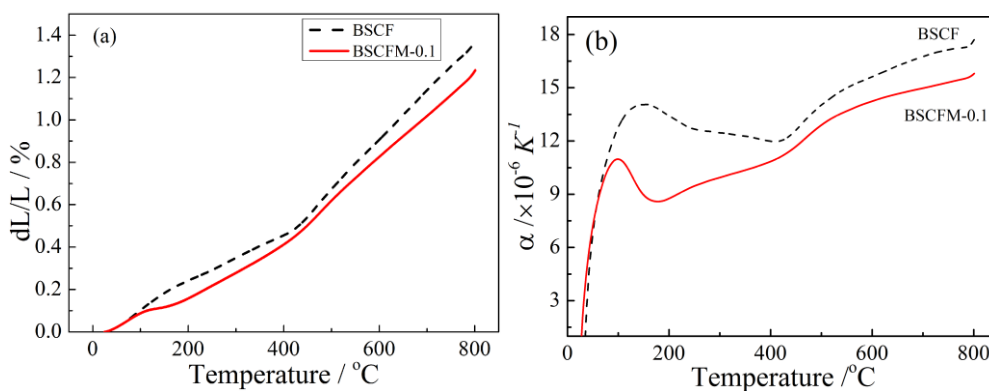


Figure 4. Thermal expansion curves for BSCF and BSCFM-0.1: (a) Relative length variation; (b) TEC value.

3.4 Performance of single cell

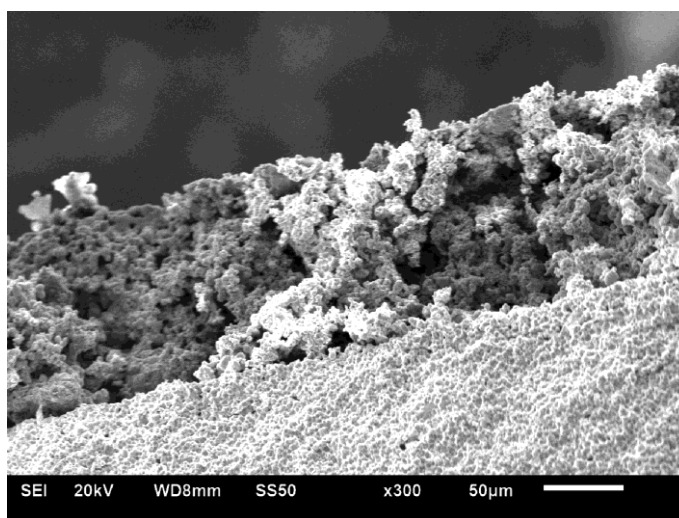


Figure 5. Cross-sectional SEM image of BSCFM-0.1 cathode on the electrolyte after sintering at $1100^\circ C$ for 2h.

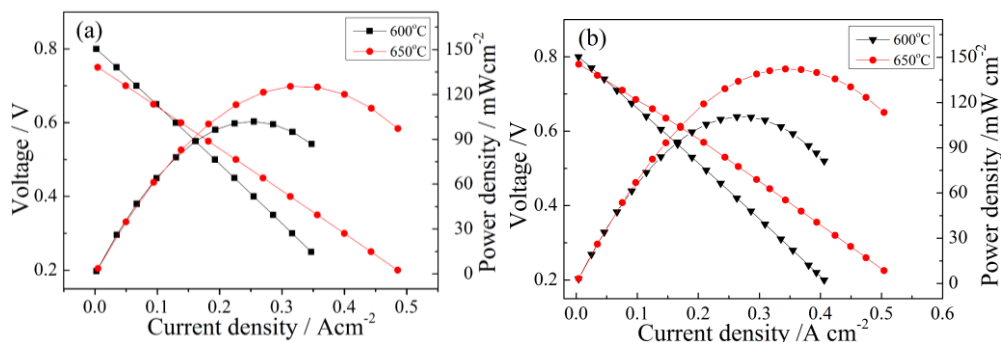


Figure 6. Performances of the Ni-LDC|LDC|cathode single cells with H₂ as the fuel and ambient air as oxidant at the 600 and 650°C using (a) BSCF; (b) BSCFM-0.1 as cathodes.

Single cell is fabricated to evaluate the performance of different cathode material under the same conditions. Figure 5 shows the cross-sectional SEM image of BSCFM-0.1 cathode layer on LDC electrolyte after co-sintering at 1100°C for 2h. The BSCFM-0.1 cathode layer is very porous, which the atmosphere can pass through easily. The electrochemical performances of a single cell were shown in Figure 6. The cell with BSCF cathode show the maximum power densities of 102 mW cm⁻² at 600°C and 125 mW cm⁻² at 650°C in Figure 6(a), while the cell with BSCFM-0.1 cathode has the relative higher values of 110 mW cm⁻² at 600°C and 142 mW cm⁻² at 650°C in Figure 6(b). Comparing with our electrolyte-supported fuel cell, Kim et al. reported that the anode-supported cell with BSCF cathode shows the high output power density of 220 mW cm⁻² at 650°C [17]. This high power density of the cell is attributed to thin electrolyte with low ohmic loss [27]. As to B-site doping of BSCF perovskite, Zr was taken to replace the Co in order to increase structural stability but decrease the electrical conductivity of Ba_{0.5}Sr_{0.5}(Co_{0.6}Zr_{0.2})Fe_{0.2}O_{3-δ} [28]. Ti was used to partial replacement the B-site of BSCF, materials of Ba_{0.5}Sr_{0.5}(Co_{0.8}Fe_{0.2})_{1-x}Ti_xO_{3-δ} were increased in chemical stability but bad in electrochemical properties [29]. In our manuscript, the same thickness (~1.5mm) electrolyte of a single cell was used to evaluate the performances of different cathodes. The cell performance suggests that the output power density of BSCFM-0.1 is high than that of BSCF. Generally, B-site modification of perovskite can change the lattice expansion [30]. Co-riched materials usually have high thermal expansion [10]. However, partial substitution for Co by Mn was successfully taken to improve the electrochemical and depress thermal expansion properties in BSCF materials.

4. CONCLUSIONS

The effects of Mn on structure, thermal expansion and performance for Ba_{0.5}Sr_{0.5}Co_{0.7}Fe_{0.2}Mn_{0.1}O_{3-δ} were investigated. The pure perovskite structure can be obtained when the content of Mn less than 0.1 under the calcinated temperature of 1100°C. Substitution by Mn for Co reduces the thermal expansion of Ba_{0.5}Sr_{0.5}Co_{0.8}Fe_{0.2}O_{3-δ} cathode material. The value of BSCFM-0.1 TEC is decreased to 14.24×10⁻⁶ K⁻¹ (600°C) comparing with BSCF. The small difference of thermal expansion will be good for the cathode to adhere on the electrolyte in SOFCs. This thermal matching of cell devices is helpful to extend the life in the thermal cycle. On the other hand, the reduction of

Mn⁴⁺ expands the crystal lattice to benefit the conduction of oxygen ion. The output power density of BSCFM-0.1 cell is 110 W cm⁻² at 600°C for the intermediate temperature SOFCs. These results suggest that the low expansion and suitable performance of BSCFM-0.1 is a very promising cathode for IT-SOFCs.

ACKNOWLEDGEMENTS

This work was financially supported by the National Natural Science Foundation of China (51302102, 11504121), the Natural Science Foundation of Anhui Province (1708085ME96), and the Natural Science Research Project for Colleges and Universities of Anhui Province (KJ2016A638).

References

1. D. Chen, Z. Shao, *Int. J. Hydrogen Energ.*, 36 (2011) 6948.
2. D. Xie, W. Guo, R. Guo, Z. Liu, D. Sun, L. Meng, M. Zheng, B. Wang, *Fuel Cells*, 16 (2016) 829.
3. Y. He, L. Fan, M. Afzal, M. Singh, W. zhang, Y. Zhao, J. Li, B. Zhu, *Electrochimi. Acta*, 191 (2016) 223.
4. B. Shri Prakash, N. Balaji, S. SenthilKumar, S. T. Aruna, *Fuel Cells*, 16 (2016) 617.
5. M. Arnold, T.M. Gesing, J. Martynczuk, A. Feldhoff, *Chem. Mater.*, 20 (2008) 5851.
6. M. Meffert, L. Unger, L. Grünwald, H. Störmer, S. Wagner, E. Ivers-Tiffée, D. Gerthsen, *J. Mater. Sci.*, 52 (2017) 2705.
7. H. Shiiba, C. Bishop, M. Rushton, M. Nakayama, M. Nogami, J. Kilner, R. Grimes, *J. Mater. Chem.*, 1 (2013) 10345.
8. L. Ge, W. Zhou, R. Ran, S. Liu, Z. Shao, W. Jin, N. Xu, *J. Membrane Sci.*, 306 (2007) 318.
9. Y. Fu, *Jpn. J. Appl. Phys.*, 45 (2006) 5996.
10. Z. Shao, G. Xiong, J. Tong, D. Hui, W. Yang, *Sep. Purif. Technol.*, 25 (2001) 419.
11. F. Tietz, I. Raj, M. Zahid, D. Stöver, *Solid State Ionics*, 177 (2006) 1753.
12. T. Hibino, S. Wang, S. Kakimoto, M. Sano, *Solid State Ionics*, 127 (2000) 89.
13. A. Babaei, L. Zhang, E. Liu, S. Jiang, *J. Alloy. Compd.*, 509 (2011) 4781.
14. Z. Shao, S. Haile, *Nature*, 431 (2004) 170.
15. Z. Shao, W. Yang, Y. Cong, H. Dong, J. Tong, G. Xiong, *J. Membrane Sci.*, 172 (2000) 177.
16. H. Patra, S. Rout, S. Pratihari, S. Bhattacharya, *Int. J. Hydrogen Energ.*, 36 (2011) 11904.
17. Y. Kim, P. Kim-Lohsoontorn, J. Bae, *Lohsoontornb*, 2 (2011) 929.
18. D. Li, M. Chao, J. Yu, M. Li, J. Zhang, E. Liang, *Mater. Lett.*, 86 (2012) 171.
19. D. Li, G. Zhu, Y. Zhang, Y. Yang, C. Han, *Rsc Adv.*, 4 (2014) 51653.
20. C. Niedrig, S. Taufall, M. Burriel, W. Menesklou, S. Wagner, S. Baumann, E. Ivers-Tiffée, *Solid State Ionics*, 197 (2011) 25.
21. F. Wang, T. Nakamura, K. Yashiro, J. Mizusaki, K. Amezawa, *Phys. Chem. Chem. Phys.*, 16 (2014) 7307.
22. R. Shannon, *Acta Crystallogr. A*, 32 (1976) 751.
23. S. Li, L. Zhe, B. Wei, X. Huang, J. Miao, G. Cao, R. Zhu, W. Su, *J. Alloy. Compd.*, 426 (2006) 408.
24. Z. Li, B. Wei, Z. Lü, X. Zhu, X. Huang, Y. Zhang, Z. Guo, W. Su, *Fuel Cells*, 12 (2012) 52.
25. S. Li, Z. Lü, X. Huang, B. Wei, W. Su, *Solid State Ionics*, 178 (2007) 417.
26. K. Eguchi, T. Setoguchi, T. Inoue, H. Arai, K. Eguchi, T. Setoguchi, T. Inoue, H. Arai, *Solid State Ionics*, 52 (1992) 165.
27. J. An, Y. Kim, T. Gür, J. Park, F. Prinz, *Nano Lett.*, 13 (2013) 4551.
28. X. Meng, B. Meng, X. Tan, N. Yang, Z. Ma, *Mater. Res. Bull.*, 44 (2009) 1293.

29. L. Bi, E. Fabbri, E. Traversa, *Solid State Ionics*, 214 (2012) 1.

30. H. Wang, C. Tablet, W. Yang, J. Caro. *Mater. Lett.*, 59 (2005) 3750.

© 2018 The Authors. Published by ESG (www.electrochemsci.org). This article is an open access article distributed under the terms and conditions of the Creative Commons Attribution license (<http://creativecommons.org/licenses/by/4.0/>).